AIAA SciTech Forum
9 - 13 January 2017, Grapevine, Texas
55th AIAA Aerospace Sciences Meeting

10.2514/6.2017-0088

Check for updates

Periodic forcing of a shock train in Mach 2.0 flow

Robin L. Hunt* , James F. Driscoll† , and Mirko Gamba‡
University of Michigan, Ann Arbor, MI 48109

High-speed schlieren movies and pressure measurements are collected to analyze the response of a shock train due to downstream forcing. The shock train is generated in a Mach 2.0 ducted flow and controlled by a downstream butterfly valve. Cyclic opening and closing of the valve (at rates up to 10 Hz) leads to oscillations in back pressure measured at the end of the duct. Subsequently, the shock train oscillates between two locations in the duct, traveling at speeds up to 3.5 m/s. Different cases with varied forcing frequency and magnitude of back pressure change are studied. For each case we evaluate the response of the back pressure and shock location by quantifying the magnitude of change, rise time, delay time, and maximum rate of change. Some of the key results include: 1) there is a linear relationship between the magnitude of the shock displacement and the back pressure change that is independent of the forcing parameters; 2) the leading shock in the shock train responds to forcing ≈6 ms after the back pressure starts to change indicating an upstream propagating disturbance; 3) the rise time of the back pressure and leading shock location are approximately the same.

Downloaded by UNIVERSITY OF MICHIGAN on April 5, 2018 | http://arc.aiaa.org | DOI: 10.2514/6.2017-0088

Nomenclature

W	Test section width (57.2 mm)
H	Test section height (69.83 mm)
x	Coordinate in the streamwise direction (mm)
y	Coordinate in the transverse direction (mm)
z	Coordinate in the vertical direction (mm)
t	Time (s)
Ω	Forcing frequency (Hz)
Θ	Control valve angle (degrees)
Θ_1	Control valve angle in the downstream state (degrees)
Θ_2	Control valve angle in the upstream state (degrees)
$p(x)$	Pressure measured at streamwise location x (kPa)
p_b	Back pressure, $p_b = p(x = 954mm)$ (kPa)
x_1	Streamwise location of the first shock (mm)
T_Θ	Rise time of the valve (s)
T_{x1}	Rise time of the leading shock response (s)
T_{pb}	Rise time of the back pressure response (s)
τ_{x1}	Time delay of the leading shock response (s)
τ_{pb}	Time delay of the back pressure response (s)
$\max(X)$	Maximum value of X (units of X)
$\min(X)$	Minimum value of X (units of X)
X'	Fluctuation component of X (units of X)
$\dot{X}$	Rate of change of X in time (units of X/s)
ΔX	Magnitude of change in X between states, e.g., $\Delta\Theta = \Theta_1 - \Theta_2$ (units of X)
$PSD(X)$	Power spectral density of X (units of X^2/Hz)

Superscripts

*Graduate Research Assistant, Dept. of Aerospace Engineering, AIAA member.
†Arthur B. Modine Professor, Dept. of Aerospace Engineering, AIAA member.
‡Assistant Professor, Dept. of Aerospace Engineering, AIAA member.

Copyright © 2017 by Robin L. Hunt, James F. Driscoll, Mirko Gamba. Published by the American Institute of Aeronautics and Astronautics, Inc., with permission.

+	Transition from the downstream to upstream state
−	Transition from the upstream to downstream state

I. Introduction

A. Overview

A shock train is a highly three-dimensional system of shock and compression waves that gradually decelerates a supersonic flow. In high-speed air-breathing engines, such as ramjets and scramjets, these fluid systems are critical to slowing and compressing captured air prior to the combustor. In a stable configuration, the pressure rise from the combustor sustains the shock train within the isolator. However, if the back pressure is too large for the shock train to compensate for, then the shock system propagates upstream until it is disgorged from the inlet. This transient process is known as inlet unstart. When the shock train is ejected, a bow shock forms outside of the inlet leading to flow spillage and reduced mass flow rate through the engine. As a consequence, there is loss of engine thrust, significantly increased loads, and intense oscillatory flow.[1–3]

In this paper we will discuss how the shock train responds to periodic forcing. That is, we will study the dynamics of the shock train when the back pressure is oscillated with magnitudes low enough that inlet unstart is avoided. During the typical operation of a high-speed air-breathing engine within the flight envelope, the combustor undergoes different transient combustion processes. For example, the initial ignition process and changes in fueling scheme (e.g., fueling rate, position, etc.) may be experienced as the vehicle follows the desired trajectory. These transient combustion phenomena induce changes in the combustor pressure and subsequently alter the shock train in the isolator such that the incoming flow conditions can be processed by the shock train to match the new combustor conditions. It is important to understand the dynamics of shock trains when perturbed by downstream forcing, such as the pressure rise from the combustor, in order to better predict and prevent unstart, and offer insight for engine control.

Shock trains exhibit complicated dynamics even when the boundary conditions are held nominally constant. The shock train position is inherently unsteady and the position fluctuations become more significant as the inflow Mach number is increased. Previous studies at higher Mach numbers have shown that the position fluctuations can be over a tunnel height away from the average location.[4–6] In addition, the movement of the shock train is coupled with pressure oscillations, which may generate detrimental noise or fluctuating wall loads. The existence of the shock train inherent unsteadiness leads us to define this mode of operation as *quasi-steady state*. To date, much about the unsteady aspect of shock trains is not understood, including the fundamental physics that drive the unsteadiness. In our ongoing work, we are studying how and why the shock train system is unsteady with constant inflow and outflow conditions. The broad goal of this work is to develop a better understanding of the flow physics so that ultimately we can reduce the unsteadiness and thus increase the operating margin of the engine. Thus far, experimental measurements have shown two perturbations through the shock train system: (1) a perturbation associated with low-frequencies that originates downstream of the shock train and propagates upstream through the boundary layer; (2) a perturbation associated with higher frequencies that originates within the shock train and emanates outwards from the source. In this paper, we use low-frequency downstream forcing as a way to mimic the former perturbation. Thus, we can compare the low magnitude perturbation from the inherent unsteadiness cases to the large disturbance generated by downstream back pressure forcing in order to gain insight on the unsteady dynamical system.

B. Previous research on shock train forcing

Experimentally, downstream forcing has been applied primarily to determine optimal methods for detecting the shock train leading edge using wall pressure measurements.[7–9] This information can be used to develop active control methods or determine the effectiveness of passive methods. Such studies on stabilizing and controlling the shock train position have used devices including suction slots,[10] vortex generators,[11] and mass injection.[12] In these cases the back pressure steadily increases and the flow remains started.

Few studies have examined the detailed shock motion induced by back pressure forcing. Hoeger et al.[13] used a 2-D transient computational model to compare the propagation of the shock train in Mach 1.8 flow due to different back pressure forcing rates. They found that when a large instantaneous back pressure is applied, the shock train first propagates upstream (against the incoming flow) with speeds up to 300 m/s.

Downloaded by UNIVERSITY OF MICHIGAN on April 5, 2018 | http://arc.aiaa.org | DOI: 10.2514/6.2017-0088

The shock train overshoots and then travels back downstream to its final rest position at up to 20 m/s. Decreasing the magnitude of the back pressure change reduces the shock train speed and the amount of overshoot. In comparison, when the back pressure change is applied more gradually (at 8,500 kPa/s) the computational model predicts a maximum speed of 110 m/s as the shock rain travels monotonically upstream to the same rest location with no overshoot.

In our previous work we conducted a preliminary study on the shock train response to back pressure forcing that was presented at the AIAA Scitech Forum in 2016.[14] In this work, forcing was imposed on the shock train system by oscillating a downstream control valve. At the time, forcing was limited to 4 Hz oscillations and the valve angle could not be directly measured or verified. High-speed schlieren imaging was used to track the location of the leading shock as the shock train responded to oscillatory downstream forcing. The schlieren field of view was small and thus the magnitude of back pressure change was small in order to visualize the leading shock at all times. We found that the shock train oscillates between an upstream and downstream location at the same frequency of the imposed back pressure oscillations. Also, the shock train transitions between the upstream and downstream locations slowly ($\approx$ 1 m/s) compared to the speed of the shock inherent unsteadiness (up to 15 m/s). A single low-speed pressure transducer was used to compare the response of the downstream portion of the shock train to the upstream location of the shock train (i.e., the leading shock location). The long response time of the transducer led us to (incorrectly) conclude that the leading shock responds to forcing prior to the change in downstream pressure. The preliminary study was a good first attempt at identifying the cyclic motion of the shock train due to oscillatory forcing but the limited diagnostics led to misleading results.

In the current work we expand and correct parts of our preliminary study discussed above. Several improvements to the diagnostics are made including: 1) use of an optical shaft encoder to measure the angle of the control valve and verify the downstream forcing mechanism; 2) increased size of the schlieren field of view in order track the leading shock location for large back pressure changes; 3) use of high-speed pressure measurements to better quantify the response time of the system. Measurements are taken over a wider range of back pressure forcing cases because we are able to impose larger changes in back pressure at higher forcing frequencies.

C. Objectives of the current research

The goal of the current work is to determine the details of how the shock train reacts to oscillatory forcing. Shock trains are complex systems, so the experiments described in this paper are designed to simplify the problem in order to better identify the underlying physics. The specific objectives are the following:

1. Fully characterize the forcing mechanism imposed by an oscillating control valve.
2. Compare the magnitude of back pressure change to the resulting displacement of the leading shock.
3. Quantify the amount of time between the onset of valve motion and the onset of back pressure change and shock displacement in order to determine which part of the system responds first.
4. Evaluate how long it takes the system to fully respond to downstream forcing.
5. Quantify the speed of the leading shock of the shock train and the rate of change of back pressure during forcing.
6. Evaluate the trajectory of the leading shock compared to the changing back pressure.

Ultimately, we want to understand how the following aspects impact the dynamics of the shock train: forcing frequency, magnitude of back pressure change, and the rate of change of back pressure. These parameters are different ways of modeling simple disturbances that could be generated by a combustor. A better understanding of the shock train response to disturbances could allow us to better predict, prevent, and control unstart.

II. Experimental Setup

A. Wind tunnel facility

The current experiments are performed in a suction type wind tunnel at the University of Michigan. A schematic diagram of the wind tunnel is shown in figure 1. Air enters the wind tunnel intake and then

Downloaded by UNIVERSITY OF MICHIGAN on April 5, 2018 | http://arc.aiaa.org | DOI: 10.2514/6.2017-0088

Nominal Mach number	2.0
Flow speed, m/s	505
Unit Reynolds number, m^{-1}	1.4×10^{7}
Stagnation pressure, kPa	98.1
Stagnation temperature, K	294
Static pressure, kPa	11.91
Static temperature, K	160
Density, kg/m^3	0.28
Viscosity, N-s/m^2	1.11×10^{-5}

Table 1. Summary of test section free stream inflow conditions.

Downloaded by UNIVERSITY OF MICHIGAN on April 5, 2018 | http://arc.aiaa.org | DOI: 10.2514/6.2017-0088

passes through a flow conditioning section containing honeycomb meshes. A one-sided converging-diverging nozzle is used to produce a nominal freestream Mach number of 2.0 in the test section of the wind tunnel. The low-aspect ratio test section has a constant, rectangular cross-section measuring 57.2 mm × 69.8 mm ($W \times H$). A right-handed coordinate system is used for this work. The x coordinate direction is oriented streamwise with $x = 0$ at the throat of the nozzle. The z-direction is normal to the bottom-wall. The origin is located on the lower right corner of the duct cross-section as one looks downstream.

The effective inflow conditions of the Mach 2.0 supersonic flow are summarized in table 1. The nominal Mach number was verified using Pitot pressure measurements. The freestream flow speed was measured using stereoscopic particle image velocimetry.[15] The stagnation pressure and temperature are determined prior to every run by measuring the room conditions. In addition, the inflow static pressure is measured during every run with a MKS 626C Baratron at location ⓐ in figure 1. This manometer is downstream of the diverging portion of the nozzle and within the constant area cross-section. The manometer accuracy is 0.25% of the reading and the response time is about 0.2 ms. The remaining parameters in table 1 that are not directly measured are estimated using the isentropic flow relations for the given Mach number.

B. Description of the shock train forcing scheme

A shock train is produced by partially closing a butterfly valve separating the diffuser to the vacuum chamber. Here, we refer to this valve as the *control valve* of the wind tunnel. The reduced area for airflow increases the pressure in the diffuser and downstream portion of the test section. A shock structure is formed in the test section to match the pressure increase. The valve angle is monitored using an optical incremental encoder that translates the rotary motion of the valve shaft into a two-channel digital output in quadrature. The resolution of the encoder is 20,000 steps per one 90° rotation.

Two pressure transducers are used to monitor the pressure rise at the end of the test section: 1) a MKS 626C Baratron capacitance manometer at $x = 1021$ mm with a response time of 0.2 ms; 2) a fast responding Kulite XCS-062 pressure gauge at $x = 954$ mm (see location ⓑ in figure 1) with a response time of 40 μs. The pressure measured by the fast responding Kulite is defined as the *back pressure* of the shock train, p_b.

Downstream forcing is introduced by periodically changing the valve angle and thus changing the back pressure. An example time trace of the valve angle is shown in figure 2. For every run a shock train is first stabilized in the test section by partially closing the control valve to an initial angle Θ_1 and establishing a desired back pressure $p_b(\Theta_1)$. Then, the valve is closed to a new angle Θ_2, resulting in a new back pressure $p_b(\Theta_2)$. After a designated time Δt, the valve opens back to the initial position Θ_1 for a time Δt. This opening/closing process is repeated at a frequency Ω for several cycles. The location (i.e., the length of the shock train) is dependent on the downstream pressure. Thus, in response to the change in valve angle, the leading shock oscillates between two positions in the test section.

Twenty-six runs have been collected to analyze the shock train response to downstream forcing. The forcing frequency is varied between 0.5–10 Hz and the magnitude of the valve angle change is varied between 0.37–1.83°. The conditions for each run are summarized in table 2.

Run	$\Delta\Theta$, deg	Ω, Hz	Run	$\Delta\Theta$, deg	Ω, Hz
0	1.48	0.50	13	0.79	9.99
1	1.48	1.00	14	0.49	2.00
2	1.45	3.33	15	0.43	5.02
3	1.48	1.99	16	1.83	5.00
4	1.33	4.97	17	0.37	7.14
5	1.11	7.13	18	1.55	7.13
6	0.86	9.99	19	1.35	1.00
7	1.36	0.51	20	1.32	1.01
8	1.35	1.00	21	1.35	1.00
9	1.35	2.00	22	1.36	0.50
10	1.31	3.33	23	1.35	2.00
11	1.19	4.97	24	0.49	2.00
12	1.00	7.14	25	1.29	3.33

Table 2. Summary of run conditions.

Downloaded by UNIVERSITY OF MICHIGAN on April 5, 2018 | http://arc.aiaa.org | DOI: 10.2514/6.2017-0088

C. Cinematographic schlieren imaging

The wind tunnel side-walls are replaced with Borosilicate glass pieces for optical access along the entire length of the test section. A z-type schlieren setup with a horizontal knife-edge is used to capture vertical density gradients in the flow. The light source was fabricated in-house and uses a high brightness LED (Luminus SBR-70) for continuous illumination. Images are recorded with a Phantom v711 camera at a rate of 10 kHz with an exposure time of 1 μs. The camera field of view covers approximately 56 mm (i.e., 83%) of the test section height and 241 mm in the streamwise direction. The image resolution is 3.5 px/mm.

Figure 3 shows two examples of instantaneous schlieren images of the Mach 2.0 shock train. Flow is from left to right. The leading shock has a normal structure, demonstrated by the Mach stem in between two very large lambda feet. For the conditions of this experiment, the resulting Mach stem height increases and angles of the lambda feet change at higher back pressures (i.e., for longer shock trains).[15] In figure 3(a) the shock train is located downstream in the field of view. This is the starting position of the shock train when $\Theta = \Theta_1$ (see label *a* in figure 2). In figure 3(b) the shock train has moved upstream in the field of view due to an increase in back pressure (see label *b* in figure 2 where $\Theta = \Theta_2$).

The individual instantaneous schlieren snapshots are processed using a shock detection algorithm to automatically detect the streamwise position of the Mach stem triple point of the leading shock in the system. We define this position x_1, following the convention set in our previous work.[15] Thus, we are able to obtain temporal data of the leading shock streamwise position sampled at 10 kHz. An 11-point Gaussian filter with a $1/e$ full-width size of 85 μs is used to smooth the data prior to data analysis.

D. High-speed pressure measurements

Simultaneously, high-speed pressure measurements are taken with five Kulite XCS-062 high sensitivity absolute pressure transducers mounted flush with the bottom-wall the test section. The gages have a pressure range of 103 kPa and a diaphragm resonance frequency of approximately 200 kHz in a cylindrical housing of 1.7 mm diameter. The Kulite signals are amplified, low pass filtered at 50 kHz, then sampled at 500 kHz.

As mentioned previously, one Kulite transducer is located at $x = 954$ mm and measures the back pressure. The other four Kulites are mounted in the bottom-wall plug (see figure 1). The bottom-wall plug contains 40 pressure ports where the Kulite transducers can be positioned in any arbitrary combination. The remaining ports are filled with blank housings. The pressure ports are located along the centerline, $y = W/2$, and are spaced 11 mm apart for high spatial-resolution results.

III. Results

A. Characterization of the valve forcing

As described in the previous section, forcing is introduced by oscillating the angle of the control valve between values of Θ_1 and Θ_2. In this section we will describe the motion of the valve in detail. In particular, we will consider how fast the valve angle changes and the total amount of time it takes to transition between angles Θ_1 and Θ_2 for different cases. This is a critical step to understand how the shock train responds in relation to the change in valve angle.

Figure 4 compares the time history of the valve angle as it increases and decreases for run 18. The blue line represents the transition from $\Theta_2 \rightarrow \Theta_1$ (i.e., as p_b is reduced) and the orange line represents the opposite transition ($\Theta_1 \rightarrow \Theta_2$, i.e., as p_b is increased). Note that the valve angle on the y-axis is normalized from 0 to 1. When $\Theta = \Theta_1$ the normalized valve angle is 0 and when $\Theta = \Theta_2$ the normalized valve angle is 1. The direction of the y-axis is reversed for the downstream to upstream transition in order to directly compare the time histories. Figure 4 demonstrates that the time history of the valve angle is the same regardless of which direction the valve is moving. Thus, the amount of time to open and close are the same for a given run. For run 18 (shown in the figure) it takes 70 ms for the valve to move 1.55°. The identical valve angle time histories allow us to directly compare the response of the shock train system as it moves upstream and downstream because the forcing mechanism is the same.

The time rate of change of the valve angle (i.e., the valve speed) is calculated from the time-history measurements of valve angle as the central difference between values. For example, figure 5 plots the valve speed, $\dot{\Theta}$, for run 18. As expected, the direction of the transition does not significantly impact the time trace of the valve speed. For the case shown (run 18), the maximum valve speed for both transitions is approximately 43°/s.

Figure 6 compares the time history of the valve angle for runs 18 and 19. Run 18 (blue line) has a higher forcing frequency and slightly higher magnitude of valve angle change than run 19 (orange line). Notice that it takes the valve longer to transition between states in run 19. Run 19 also has a significantly longer amount of time at a constant valve angle due to the low forcing frequency. Despite these differences, both cases have a similar valve angle rate of change during the first part of the transition. For each cycle the points of maximum and minimum rate of change (as the valve opens and closes, respectively) are identified with circular symbols. Note that the valve angle changes the fastest near the beginning on the cycle. The absolute value of the maximum rate of change is 46°/s and 35°/s for runs 18 and 19, respectively.

In our experiment the magnitude of the valve angle change ($\Delta\Theta$) and the forcing frequency (Ω) are independent variables. Given these user inputs to the system the valve transitions between states with a certain speed and rise time. The valve rise time, T_Θ, is defined as the time it takes for the valve to transition from its original angle to 95% of the final angle. Figure 7(a) demonstrates a linear relationship between the rise time and the forcing frequency for different cases of $\Delta\Theta$. Higher forcing frequencies are associated with smaller rise times. Figure 7(b) shows that there is a linear relationship between the maximum valve speed and the magnitude of the valve angle change for different cases of Ω. Large amplitude changes in the valve angle lead to increased valve speeds. However, due to the relatively low-speed motion of the valve, the magnitude of the valve angle change is restricted to smaller values at high forcing frequencies. Thus, we cannot impose forcing with both high frequencies and large valve angle displacements. In addition, the valve speeds obtained in our experiments are slow compared to other experiments in the literature.[1,13] Therefore, we are generating a more gradual downstream pressure change.

B. Description of the pressure and shock system response to forcing

The change in valve angle sends disturbances upstream through the diffuser that ultimately effect the shock train. Within the test section we measure multiple responses: 1) the back pressure (p_b) measured at the end of the test section, 2) the pressure (p) at discrete locations along the length of the shock train, and 3) the location of the leading shock (x_1). As an example, we will discuss figures 8(a) and 8(b) that compare the time trace of valve angle to leading shock position and pressure, respectively, for a portion of run 19. In the figure, there are three distinct regions of time where the valve angle is constant: $0.30 < t < 0.52$, $0.69 < t < 1.02$, and $1.16 < t < 1.40$ seconds.

For $0.30 < t < 0.52$ seconds the valve angle is at $\Theta = \Theta_1$ and the leading shock is located downstream at $x \approx 700$ mm as seen in figure 8(a). The shock position is nominally constant but small fluctuations are evident

Downloaded by UNIVERSITY OF MICHIGAN on April 5, 2018 | http://arc.aiaa.org | DOI: 10.2514/6.2017-0088

in the time trace due to an inherent unsteadiness in the shock train system. Our previous studies[15] with this experimental setup have shown that with a nominally constant back pressure the position fluctuations can reach up to 20 mm away from the mean position. However, 98% of the position fluctuations are within 10 mm of the average location. These statistics are consistent with the unsteadiness of the leading shock in the forcing cases during periods of time when the valve angle is constant. Next, consider the pressure traces plotted in figure 8(b) for $0.30 < t < 0.52$ seconds. The transducers located at x=620 mm and x =718 mm (the purple and dark blue curves) are upstream of the shock train and thus measure a pressure nominally equal to the inflow static pressure during $0.30 < t < 0.52$ seconds. The three downstream transducers (light blue, green, and yellow curves) measure the pressure at different points along the shock train length. The pressure measurements taken along the shock train length exhibit small fluctuations during $0.30 < t < 0.52$ seconds due to the inherent unsteadiness of the shock system and the generation of turbulence from the shock train. The average values of the leading shock location and each pressure measurement during $0.30 < t < 0.52$ seconds are used to define the *downstream state* of the shock train system. That is, when the shock train is located downstream the shock train system is characterized by these properties.

At $t = 0.52$ seconds the valve angle starts to decrease (i.e., the valve begins to close). As a result the measured pressures increase and the shock train is pushed upstream. As seen in figure 8(b), the back pressure begins to rise after a time delay, τ_{pb}^{-}. The "-" superscript indicates that the valve angle is decreasing. The back pressure time delay is mathematically defined as the first value in the time series where

$$\frac{p_b - \min(p_b)}{\max(p_b) - \min(p_b)} < 0.95 \tag{1}$$

Similarly, the shock train responds to the change in valve position after a time delay, τ_{x1}^{-} (see figure 8(a)). The leading shock time delay is mathematically defined as the first value in the time series where

$$\frac{x_1 - \min(x_1)}{\max(x_1) - \min(x_1)} < 0.95 \tag{2}$$

Notice that as the leading shock transitions to an upstream position the time trace still contains small fluctuations due to the system inherent unsteadiness.

By $t = 0.69$ seconds the valve angle is at $\Theta = \Theta_2$. Soon after, the leading shock is located at a nominally constant upstream position. Overall, the leading shock has moved a distance Δx_1 from the original downstream location to the new upstream location associated with the valve angle Θ_2. The leading shock rise time, T_{x1}^{-}, is defined as the time it takes for the leading shock to move 95% of Δx_1. There is no evidence of overshoot as the shock train reaches its upstream location as previous investigators have observed for faster actuation speeds.[13] Experiments and computations by Hoeger et al.[13] suggest that the overshoot is a function of the rate at which the control surface changes. Thus, the lack of overshoot in the current experiments could be due to the relatively slow valve speed. Similarly, the back pressure reaches a nominally constant value allowing us to quantify the overall change in back pressure between states, Δp_b. The back pressure rise time, T_{pb}^{-}, is defined as the amount of time it takes for the back pressure to reach 95% of Δp_b. The end of the rise time signals that pressure and shock location are nominally constant and the system has stabilized in its *upstream state*. The system will stay in the upstream state for a time dependent on the forcing frequency Ω. From figure 8 we infer that the shock train system is highly sensitive to the valve angle because the relative change in valve angle is substantially smaller than the resulting change in back pressure and shock position. In the case shown, a 2% decrease in valve angle leads to a 28% decrease in leading shock position and a 17% increase in back pressure.

At $t = 1.02$ seconds the transition process occurs in reverse to complete the cycle. That is, the valve angle increases from Θ_2 to Θ_1. In response, the shock train moves back downstream and the measured pressures decrease to match the new downstream boundary condition set by the valve. Once again, the delay times for the shock movement τ_{x1}^{+} and back pressure change τ_{pb}^{+} are quantified as the time between the start of the valve change and the start of the shock or pressure response, respectively. The rise times for the shock movement T_{x1}^{+} and back pressure change T_{pb}^{+} are defined as the time it takes for the shock location and back pressure, respectively, to transition between the upstream and downstream state. Note that a "+" superscript is now used to indicate that the valve angle is increasing.

Now, consider a portion of the time traces for a higher forcing frequency case (run 18) shown in figure 9. The leading shock position and pressure time traces are plotted in figures 9(a) and 9(b), respectively. Unlike run 19 (shown in figure 8) the shock train does not stay in a particular state for a long period of time. For

Downloaded by UNIVERSITY OF MICHIGAN on April 5, 2018 | http://arc.aiaa.org | DOI: 10.2514/6.2017-0088

instance, once the leading shock reaches its upstream position it immediately changes direction and moves back downstream.

In figure 9 only a portion of the time traces are shown. During one run the forcing cycle is repeated several times. To reduce the effects of the shock system inherent unsteadiness we average all of the cycles for a given run. The time delays ($\tau_{x1}^{\pm}$ and $\tau_{pb}^{\pm}$) and rise times ($T_{x1}^{\pm}$ and $T_{pb}^{\pm}$) discussed previously are then quantified based on the cycle-averaged curves. Figure 10 shows the cycle-average time trace of valve angle, shock position, and back pressure for run 18 (the same run shown in figure 9). For easier comparison, the time traces are normalized between 0 and 1 as follows:

$$\widehat{\Theta} = \frac{\Theta - \Theta_2}{\Theta_1 - \Theta_2} \tag{3}$$

$$\widehat{x_1} = \frac{x_1 - \min(x_1)}{\max(x_1) - \min(x_1)} \tag{4}$$

$$\widehat{p_b} = \frac{p_b - \min(p_b)}{\max(p_b) - \min(p_b)} \tag{5}$$

Thus, the minimum and maximum points of the original signal correspond to normalized values of 0 and 1, respectively. Orange lines correspond to a decrease in valve angle (i.e., downstream to upstream transition) and blue lines correspond to an increase in valve angle (i.e., upstream to downstream transition).

Additional insight on the system is obtained by examining the time rate of change of the measured properties calculated using the cycle-averaged curves. As an example, figure 11 plots the absolute values of the time rate of change of back pressure, $\dot{p_b}$, and leading shock location, $\dot{x_1}$, for run 18. In each case, the time rate of change is calculated from the time-history of the cycle-averaged measurements as the central difference between values. The orange lines correspond to a decrease in valve angle (i.e., downstream to upstream transition) and blue lines correspond to an increase in valve angle (i.e., upstream to downstream transition). Note that the resulting derivatives are essentially smoothed due to the averaging of multiple cycles. Figure 11(a) shows that for run 18, the back pressure time rate of change can reach up to 80 kPa/s. Figure 11(b) shows that the bulk motion of the leading shock can reach speeds up to 2.8 m/s for run 18.

Averaging multiple cycles during a run essentially filters out the low-magnitude, high-frequency (LMHF) components of the signal that are caused by the system inherent unsteadiness. For example, see figure 12(a) that compares the original time trace to the cycle-averaged time trace for run 6. To examine the LMHF fluctuation component of the signal the bulk motion due to forcing (i.e., the cycle-averaged time trace) is subtracted from the original time trace. An example of the resulting LMHF fluctuation time trace is seen in figure 12(b). For comparison, the fluctuation component of the quasi-steady state cases (i.e., when p_b is constant) is found by subtracting the time-average value of the shock position. Thus, we can directly compare the LMHF leading shock fluctuations during quasi-steady state (i.e., when p_b is constant) and during forcing. Figures 13(a) and 13(b) are histograms comparing the LMHF fluctuation magnitude and shock speeds, respectively, for our current example (run 6). The histograms are nearly identical for the forcing and quasi-steady state cases. In addition, figure 13(c) shows that the power spectral densities of the LMHF fluctuations are the same for forcing and quasi-steady state. Thus, the low-magnitude, high-frequency fluctuation component due to inherent unsteadiness is superimposed onto the bulk motion of the shock train when forcing is applied. We have looked at run 6 in detail but the results are the same for the other runs.

C. Comparison between shock system and back pressure responses

Thus far we have described the response of the system to a change in valve position for one case. In this section we will compare the response of the back pressure and leading shock position across all of the run conditions outlined in table 2. In particular, we will quantify the magnitude of the response, time delay, rise time, and maximum rate of change.

Figure 14 compares the magnitude of the leading shock displacement with the change in back pressure. The results are calculated using the cycle-averaged curves and thus one point is plotted for every run. An increased change in back pressure is associated with a linear increase in leading shock displacement. The linear fit crosses through the origin of the plot indicating that a zero change in back pressure is associated with no bulk shock train movement. The slope of the linear fit is 30 mm/kPa. In our previous work[15] we measured the time-average position of the leading shock at different values of constant back pressure. Thus, the shock train was in a quasi-steady state and the only variation in position was due to the system inherent

Downloaded by UNIVERSITY OF MICHIGAN on April 5, 2018 | http://arc.aiaa.org | DOI: 10.2514/6.2017-0088

unsteadiness. The resulting slope of the quasi-steady state leading shock location versus back pressure is approximately 34 mm/kPa. This value is similar to that of the current experiments and indicates that within the range of forcing conditions of this study, the leading shock displacement due to forcing can be reliably predicted without knowing forcing parameters such as Ω.

Next, we will compare the time between the onset of valve angle change and the system response for different forcing cases with $\Omega > 2$ Hz. Cases with forcing frequency less than or equal to 2 Hz are not considered in this analysis because there are not enough cycles during a run to average out the effects of the inherent unsteadiness and the time delay cannot be reliably identified. Figure 15(a) compares the delay times of the leading shock and back pressure responses. Two points are plotted for every run: 1) the cycle-averaged result for the upstream-to-downstream transition (blue circles); 2) the cycle-averaged result for the downstream-to-upstream transition (orange triangles). For reference, the gray, dotted line represents $\tau_{x1} = \tau_{pb}$. Despite some run-to-run scatter, the back pressure responds to the valve forcing prior to the leading shock movement (i.e., $\tau_{pb} < \tau_{x1}$) for every run. This indicates that the disturbance generated by the valve movement travels upstream and impacts the downstream portion of the shock train before traveling upstream to the leading shock. On average, it takes 6 ms for the disturbance to travel from x =954 mm (i.e., where the transducer measuring back pressure is located) to the leading shock location. Thus, the disturbance travels upstream through the boundary layer at a nominal rate of 50 m/s. Our previous work[16] indicated the same upstream velocity for small, low-frequency perturbations that lead to inherent unsteadiness in the shock train system. The small perturbations causing inherent unsteadiness and the large disturbance due to forcing could be propagated by the same mechanism.

Figure 15(b) compares the leading shock time delays for the different transitions. For reference, the gray, dotted line represents $\tau^+_{x1} = \tau^-_{x1}$. Notice it takes slightly longer for the disturbance to reach the leading shock when the leading shock is located upstream (i.e., $\tau^+_{x1} > \tau^-_{x1}$). This could be due to the longer distance the disturbance has to travel before it interacts with the leading shock. Unlike the shock position, we find that the back pressure time delay is not consistently higher or lower for a particular transition (see figure 15(c)). Finally, note that the time delay results discussed (i.e., cases with $\Omega > 2$ Hz) are independent of forcing parameters. Therefore, the mechanism that propagates the disturbance upstream to the leading shock is independent of Ω and $\Delta\Theta$.

Figure 16 compares the cycle-averaged rise time of the leading shock and the back pressure. Cases with forcing frequency less than or equal to 2 Hz are not considered in this analysis because there are not enough cycles during a run to average out the effects of the inherent unsteadiness and the precise rise time cannot be easily identified. Two points are plotted for every run with $\Omega > 2$ Hz: 1) the cycle-averaged result for the upstream-to-downstream transition (blue circles); 2) the cycle-averaged result for the downstream-to-upstream transition (orange triangles). For reference, the gray, dotted line represents $T_{x1} = T_{pb}$. Generally, the points fall along this dotted line indicating that the time it takes the shock to move between states is equal to the time it takes the back pressure to change for cases with $\Omega > 2$ Hz. In addition, we find no significant difference in rise times for the upstream to downstream transition compared to the downstream to upstream transition.

Thus far, we have seen that when forcing is applied the system takes a finite amount of time to change from its initial state to its final state. For forcing frequencies between 3–10 Hz the shock system moves 1–2 mm for every ms. If we assume that this finite response time is the same at higher forcing frequencies then as forcing frequency increases the shock system will have a smaller displacement. For example, let $\Omega = 500$ Hz. The valve angle decreases and starts to push the shock train upstream. The shock system has 2 ms to respond before the valve angle increases and sends the shock system back downstream. In these 2 ms the shock train system can only move 2–4 mm. Thus, the shock train does not have time to respond to high frequency disturbances that originate downstream. Figure 17 illustrates what the maximum shock train displacement is for high forcing frequencies, assuming that the response of the system remains similar to what is quantified for the range of forcing conditions of the current study.

The rise times have been discussed for high forcing frequency runs. The lower forcing frequency runs do not have enough cycles during a run to completely average out the effects of the inherent unsteadiness. However, we look at the normalized time traces to determine the general relationship between rise time and forcing frequency. For instance, figure 18 shows the cycle-average time trace of valve angle, shock position, and back pressure for run 19 (the same run shown in figure 8). The time traces are normalized between 0 and 1. Orange lines correspond to a decrease in valve angle (i.e., downstream to upstream transition) and blue lines correspond to an increase in valve angle (i.e., upstream to downstream transition). In this

Downloaded by UNIVERSITY OF MICHIGAN on April 5, 2018 | http://arc.aiaa.org | DOI: 10.2514/6.2017-0088

low frequency case, the back pressure and the leading shock location take significantly longer to transition from the downstream state to the upstream state. For example, in run 19 the leading shock takes about 20 ms to move from its upstream location to its downstream location. The transition from downstream to upstream location takes 40 ms. We hypothesize that the shock train moves slower going upstream because it is traveling against the bulk fluid motion of the freestream flow.

Finally, figure 19 compares the maximum cycle-average speed of the leading shock to the maximum cycle-average back pressure rate of change. All forcing frequencies are compared in this plot. The orange triangles are the results of the downstream to upstream transition. The blue circles are results of the upstream to downstream transition. Clearly, increasing the back pressure rate of change leads to a faster bulk motion of the shock train. Overall, the maximum back pressure rate of change measured is 110 kPa/s. Also, the bulk shock speed of the leading shock does not exceed 3.5 m/s. From our previous experiments we know the shock can fluctuate at speeds up to 15 m/s due to the system inherent unsteadiness. Comparatively, the bulk motion of the shock train is much slower.

IV. Conclusions

The properties of an oscillating shock train due to downstream forcing are studied. Forcing is introduced by changing the angle of a downstream control valve. In response to the valve closing, the back pressure (p_b) increases and the shock train is pushed to a new location in the duct, effectively changing the length of the shock train. The reverse process occurs for the valve opening. Twenty-seven cases forcing are considered to observe the effects of increasing forcing frequency and the magnitude of the valve change. These different cases are used to model different ways the back pressure could change in an actual combustor, thus inducing shock train propagation in the isolator. Some of the key results are as follows:

1. When forcing is applied a bulk motion is superimposed onto the low-magnitude, high-frequency unsteady motion of the shocks due to inherent unsteadiness.

2. There is a linear relationship between the magnitude of the shock displacement and the back pressure change that is independent of the forcing parameters. Thus, the end conditions after forcing can be estimated using results from quasi-steady state shock train studies.

3. The leading shock in the shock train responds to forcing 6 ms after the back pressure starts to change. This indicates an upstream propagating disturbance that travels through the boundary layer at approximately 50 m/s.

4. The rise time of the back pressure and leading shock location are approximately the same. At low frequencies the downstream to upstream transition has a longer rise time than the upstream to downstream transition. At high forcing frequencies the rise times for the different transitions are the same. The finite rise time means the shock train does not have time to respond to high frequency disturbances.

5. During forcing, the shock train transitions between the upstream and downstream locations at a bulk speed less than 3.5 m/s. Comparatively, the shock fluctuations due to inherent unsteadiness are much faster (up to 15 m/s). The bulk speed of the shock depends on the maximum back pressure rate of change. In our experiments the back pressure rate of change does not exceed 100 kPa/s.

Downloaded by UNIVERSITY OF MICHIGAN on April 5, 2018 | http://arc.aiaa.org | DOI: 10.2514/6.2017-0088

Acknowledgments

RLH acknowledges the financial support of the National Science Foundation Graduate Research Fellowship Program under Grant No. DGE 1256260. The authors would like to thank the valuable help of Rohan Morajkar in conducting some of the experiments presented here.

References

[1]Wagner, J. L., Yuceil, K. B., Valdivia, A., Clemens, N. T., and Dolling, D. S., "Experimental investigation of unstart in an inlet/isolator model in Mach 5 flow," *AIAA Journal*, Vol. 47, No. 6, 2009, pp. 1528–1542.

[2]Rodi, P. E., Emami, S., and Trexler, C. A., "Unsteady pressure behavior in a ramjet/scramjet inlet," *Journal of propulsion and power*, Vol. 12, No. 3, 1996, pp. 486–493.

[3]Tan, H., Li, L., Wen, Y., and Zhang, Q., "Experimental investigation of the unstart process of a generic hypersonic inlet," *AIAA Journal*, Vol. 49, No. 2, 2011, pp. 279–288.

[4]Klomparens, R. L., Driscoll, J. F., and Gamba, M., "Unsteadiness characteristics and pressure distribution of an oblique shock train," *AIAA Scitech, paper no. 2015-1519*, 2015.

[5]Sugiyama, H., Tsujiguchi, Y., and Honma, T., "Structure and oscillation phenomena of pseudo-shock waves in a straight square duct at Mach 2 and 4," *15th AIAA International Space Planes and Hypersonic Systems and Technologies Conference, AIAA paper 2008-2646*, American Institute of Aeronautics and Astronautics, 2008.

[6]Lindstrom, C. D., Davis, D., Williams, S., and Tam, C., "Shock-train structure resolved with absorption spectroscopy part II: analysis and CFD comparison," *AIAA Journal*, Vol. 47, No. 10, 2009, pp. 2379–2390.

[7]Le, D. B., Goyne, C. P., and Krauss, R. H., "Shock train leading-edge detection in a dual-mode scramjet," *Journal of Propulsion and Power*, Vol. 24, No. 5, 2008, pp. 1035–1041.

[8]Hutzel, J. R., Decker, D. D., Cobb, R. G., King, P. I., Veth, M. J., and Donbar, J. M., "Scramjet isolator shock train location techniques," *49th AIAA Aerospace Sciences Meeting including the New Horizons Forum and Aerospace Exposition, AIAA paper 2011-402*, American Institute of Aeronautics and Astronautics, 2011.

[9]Sajben, M., Donovan, J. F., and Morris, M. J., "Experimental investigation of terminal shock sensors for mixed-compression inlets," *Journal of Propulsion and Power*, Vol. 8, No. 1, 1992, pp. 168–174.

[10]Weiss, A. and Olivier, H., "Influence of a Normal Slot Boundary Layer Suction System onto a Shock Train," *28th International Symposium on Shock Waves*, edited by K. Kontis, Vol. 2, Springer Berlin Heidelberg, Berlin, Heidelberg, 2012, pp. 141–146.

[11]Valdivia, A., Yuceil, K. B., Wagner, J. L., Clemens, N. T., and Dolling, D. S., "Control of supersonic inlet-isolator unstart using active and passive vortex generators," *AIAA Journal*, Vol. 52, No. 6, 2014, pp. 1207–1218.

[12]Huang, H., Tan, H., Wang, J., Sun, S., and Ning, L., "A fluidic control method of shock train in hypersonic inlet/isolator," *50th AIAA/ASME/SAE/ASEE Joint Propulsion Conference, AIAA paper 2014-3846*, 2014.

[13]Hoeger, T. C., King, P. I., Donbar, J. M., and Cox-Stouffer, S., "2-D transient CFD model of an isolator shock train," *17th AIAA International Space Planes and Hypersonic Systems and Technologies Conference, AIAA paper 2011-2221*, 2011.

[14]Klomparens, R. L., Driscoll, J. F., and Gamba, M., "Response of a shock train to downstream back pressure forcing," *AIAA Scitech, paper no. 2016-0078*, 2016.

[15]Hunt, R. L., Driscoll, J. F., and Gamba, M., "Unsteadiness characteristics and three-dimensional leading shock structure of a Mach 2.0 shock train," *AIAA Scitech*, 2017.

[16]Hunt, R. L., Driscoll, J. F., and Gamba, M., "Evolution of unsteady pressure and shock position fluctuations in a quasi-steady shock train," .

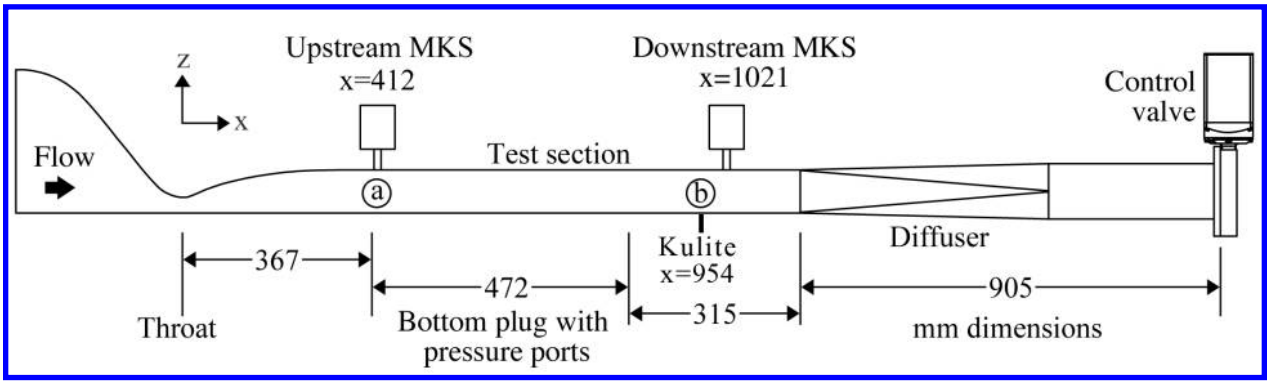

Figure 1. Schematic diagram of the wind tunnel.

Downloaded by UNIVERSITY OF MICHIGAN on April 5, 2018 | http://arc.aiaa.org | DOI: 10.2514/6.2017-0088

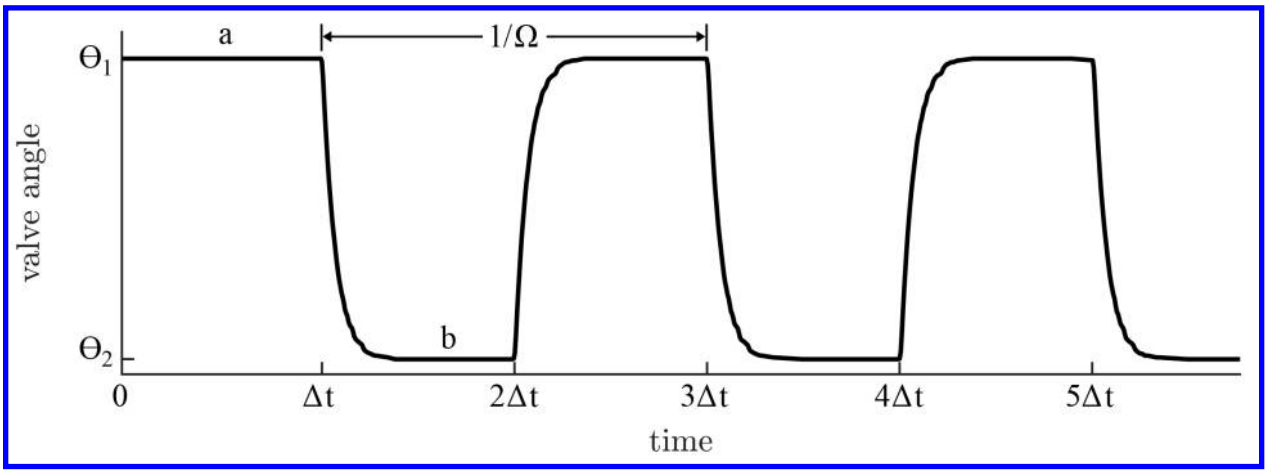

Figure 2. Example time trace of the valve angle.

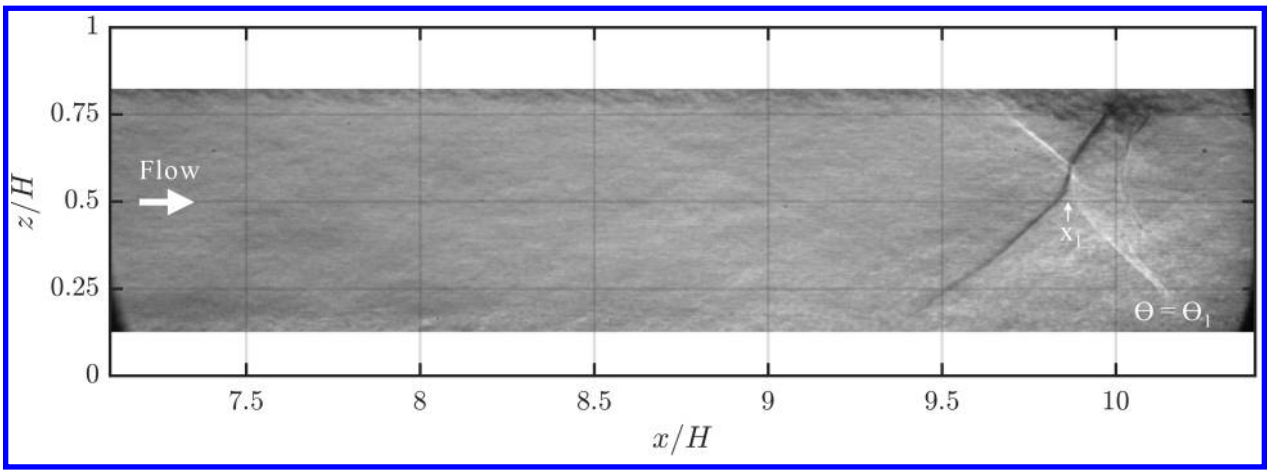

(a)

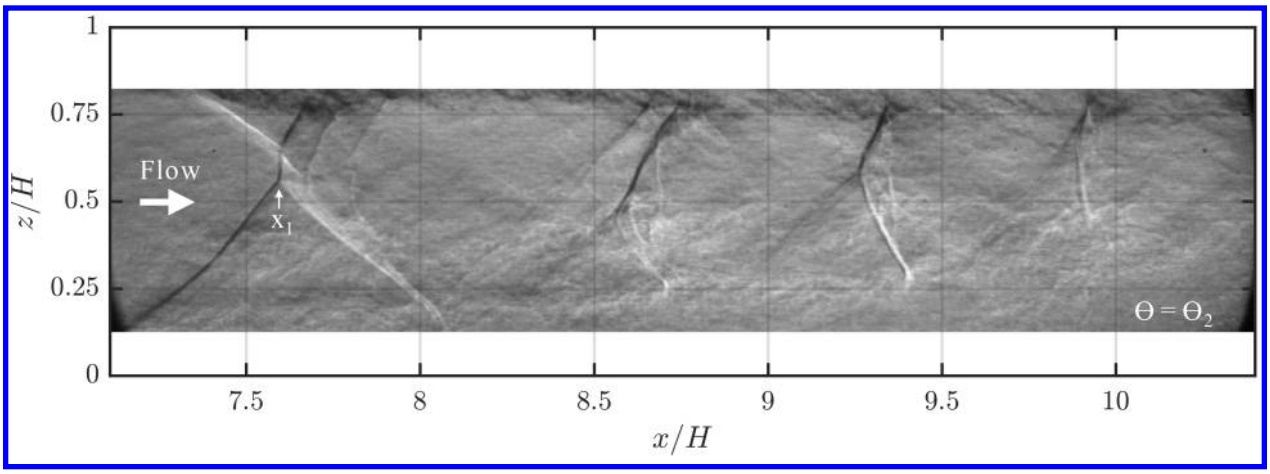

(b)

Figure 3. Instantaneous schlieren image: (a) shock train located downstream when $\Theta = \Theta_1$; (b) shock train located upstream when $\Theta = \Theta_2$.

Downloaded by UNIVERSITY OF MICHIGAN on April 5, 2018 | http://arc.aiaa.org | DOI: 10.2514/6.2017-0088

Downloaded by UNIVERSITY OF MICHIGAN on April 5, 2018 | http://arc.aiaa.org | DOI: 10.2514/6.2017-0088

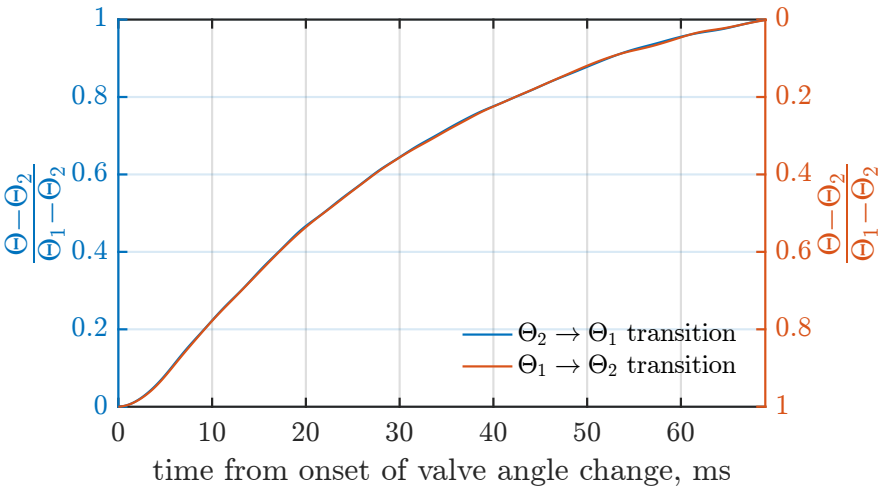

Figure 4. Comparison of valve angle time history as it is opened and closed (run 18).

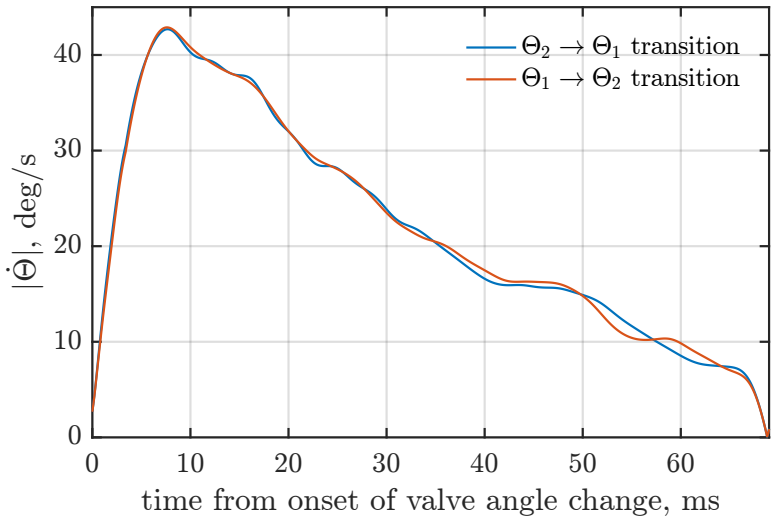

Figure 5. Time rate of change of valve angle (run 18).

Downloaded by UNIVERSITY OF MICHIGAN on April 5, 2018 | http://arc.aiaa.org | DOI: 10.2514/6.2017-0088

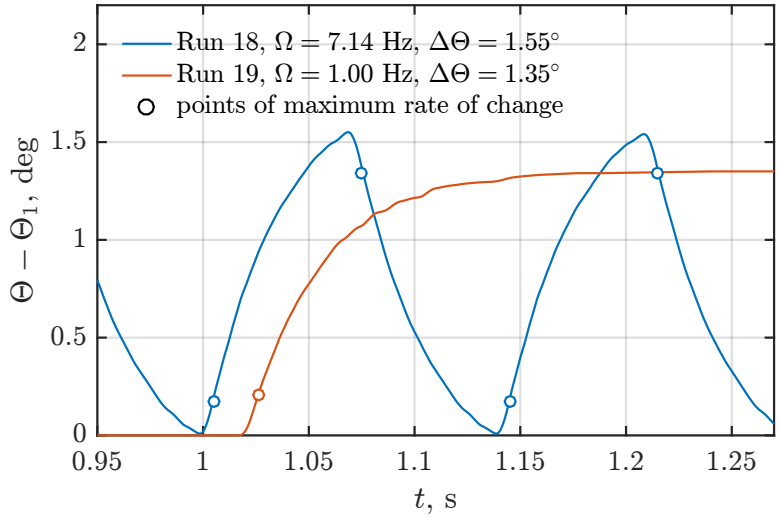

Figure 6. Comparison of valve movement for different cases (runs 18 and 19).

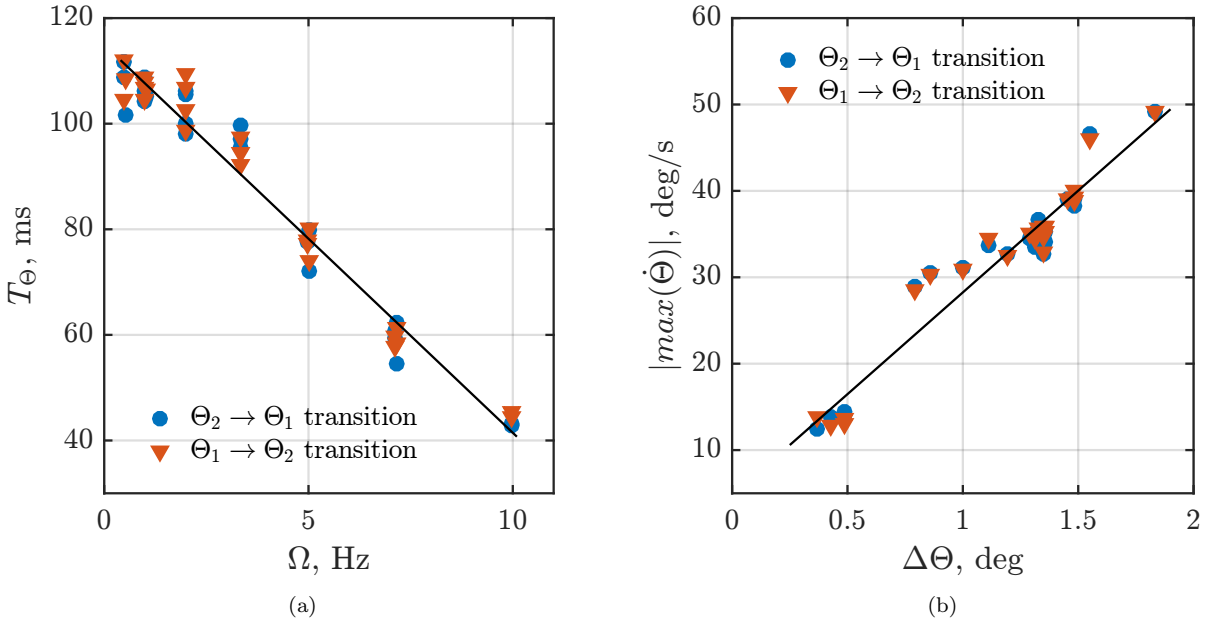

Figure 7. Characteristics of the control valve forcing: (a) rise time versus forcing frequency; (b) maximum rate of valve angle change versus magnitude of valve angle change.

Downloaded by UNIVERSITY OF MICHIGAN on April 5, 2018 | http://arc.aiaa.org | DOI: 10.2514/6.2017-0088

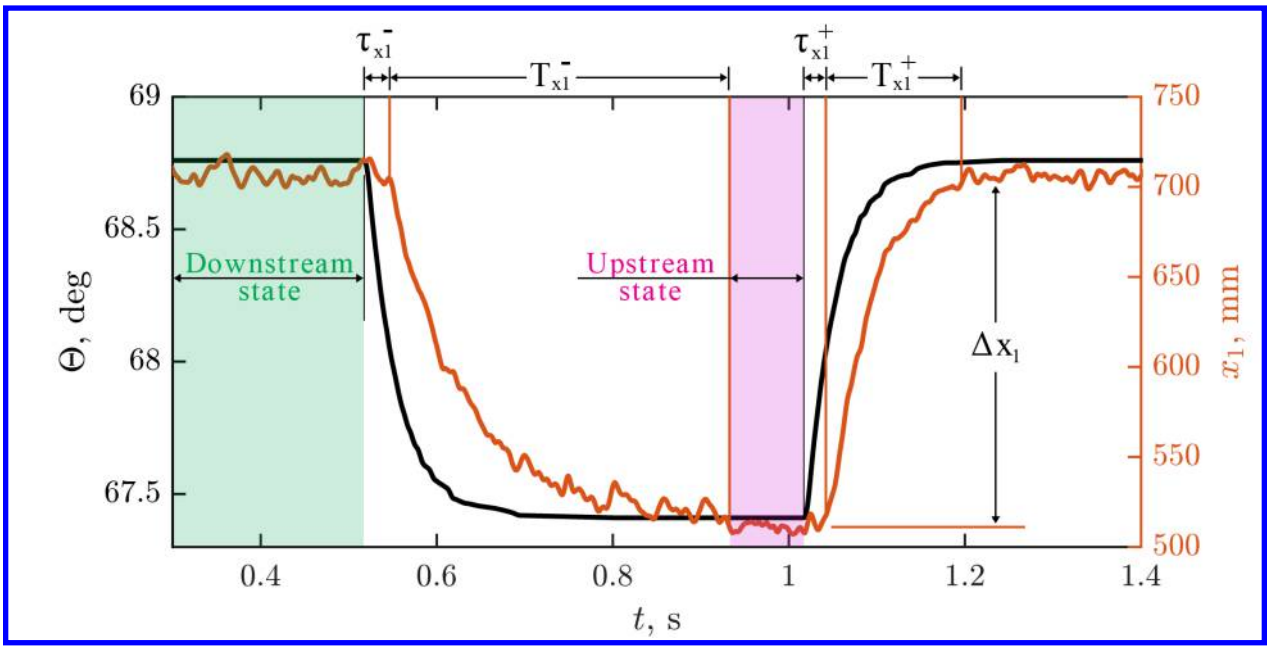

(a)

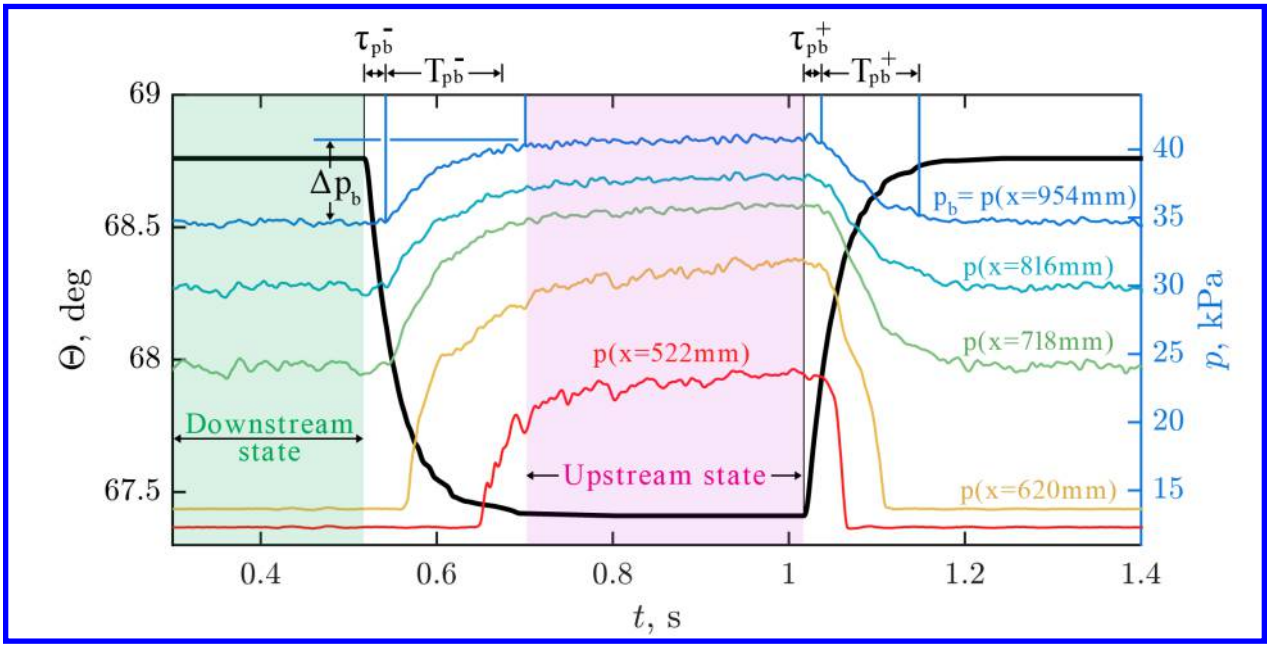

(b)

Figure 8. Example time traces demonstrating signal lags and rise times (run 19): (a) leading shock location, x_1; (b) pressure, p.

Downloaded by UNIVERSITY OF MICHIGAN on April 5, 2018 | http://arc.aiaa.org | DOI: 10.2514/6.2017-0088

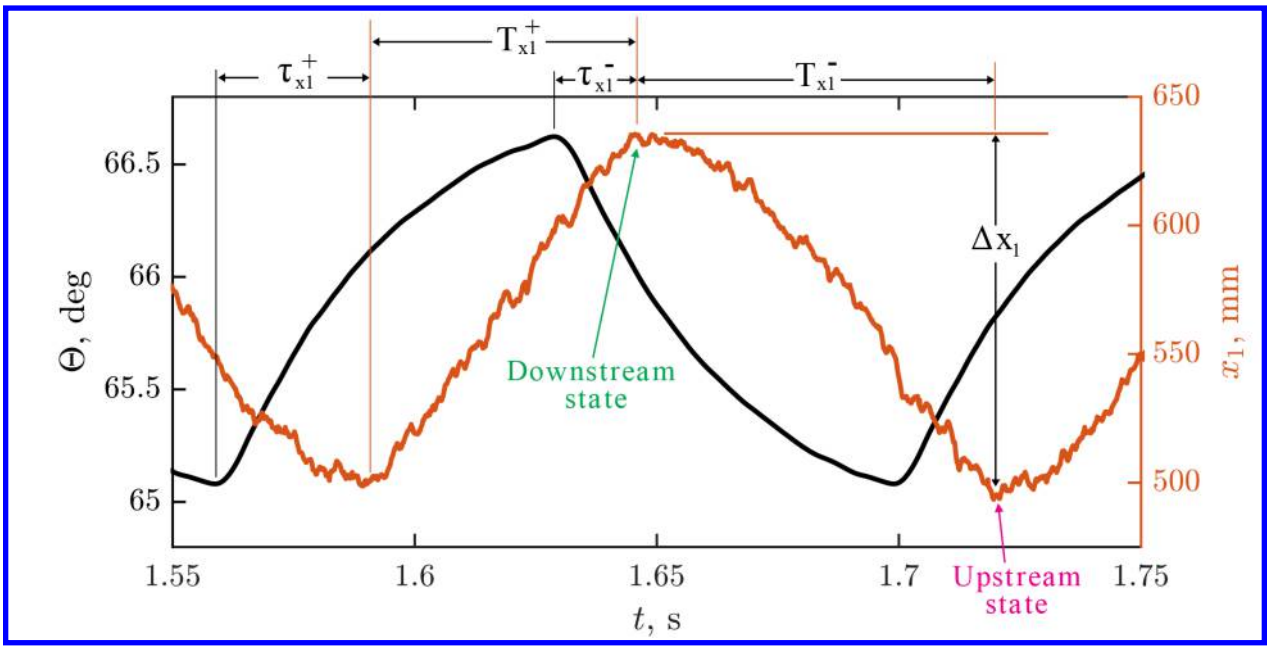

(a)

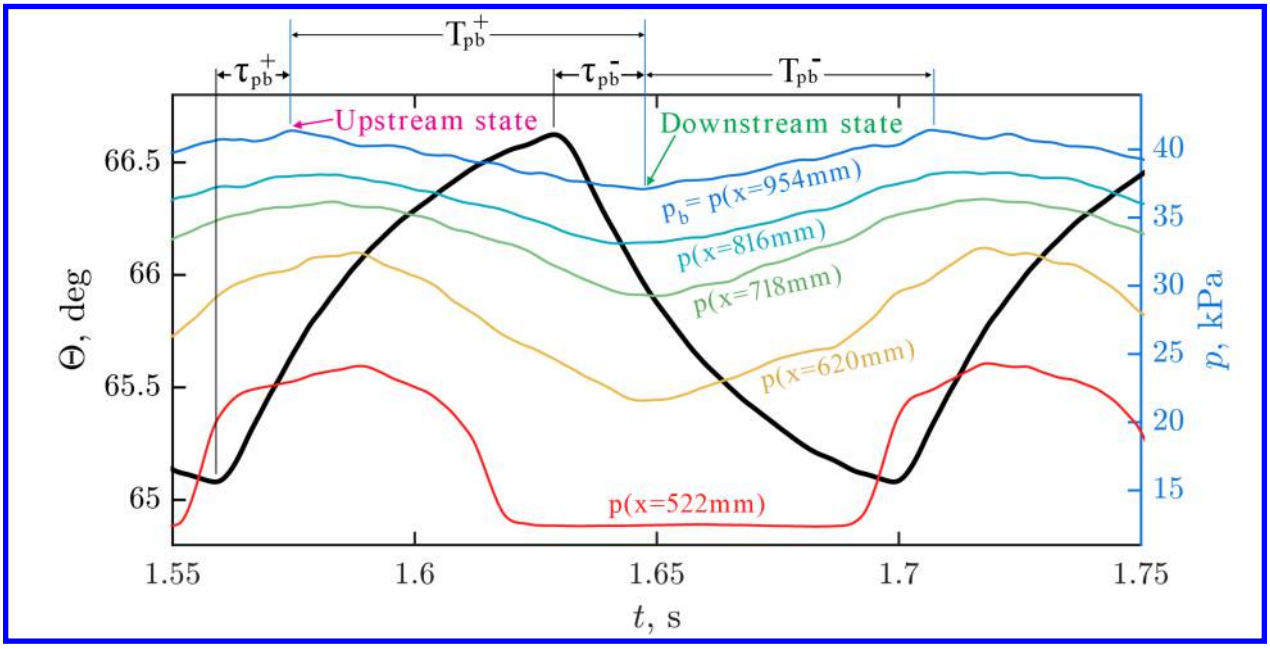

(b)

Figure 9. Example time traces demonstrating signal lags and rise times (run 18): (a) leading shock location, x_1; (b) pressure, p.

Downloaded by UNIVERSITY OF MICHIGAN on April 5, 2018 | http://arc.aiaa.org | DOI: 10.2514/6.2017-0088

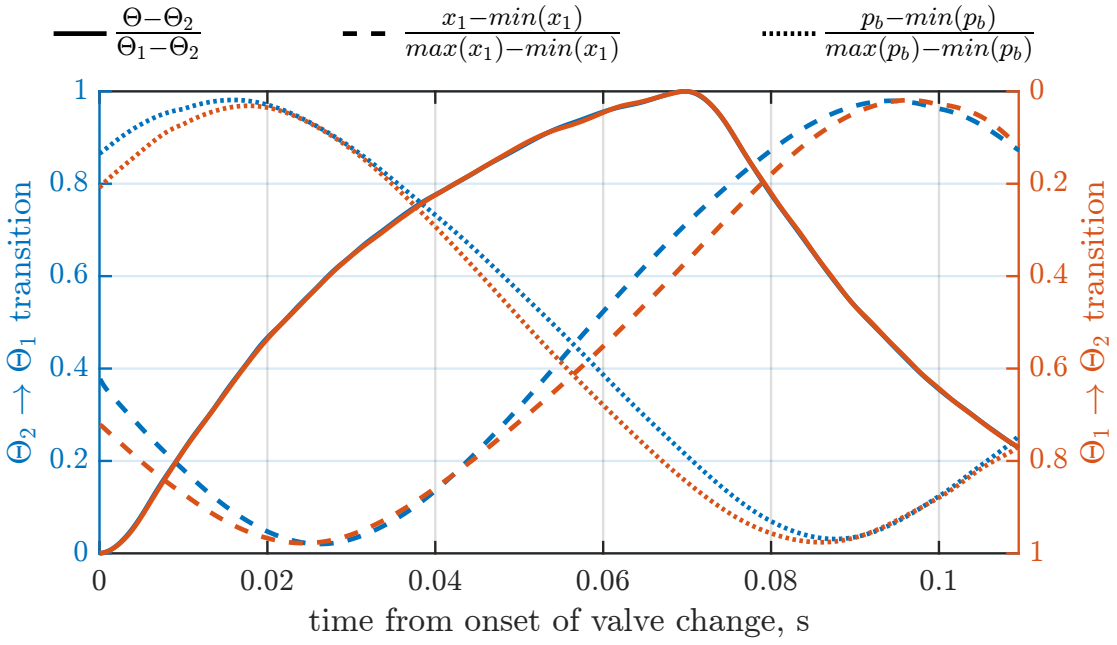

Figure 10. Normalized values of the cycle-average valve angle, shock position, and pressure during different transitions (run 18).

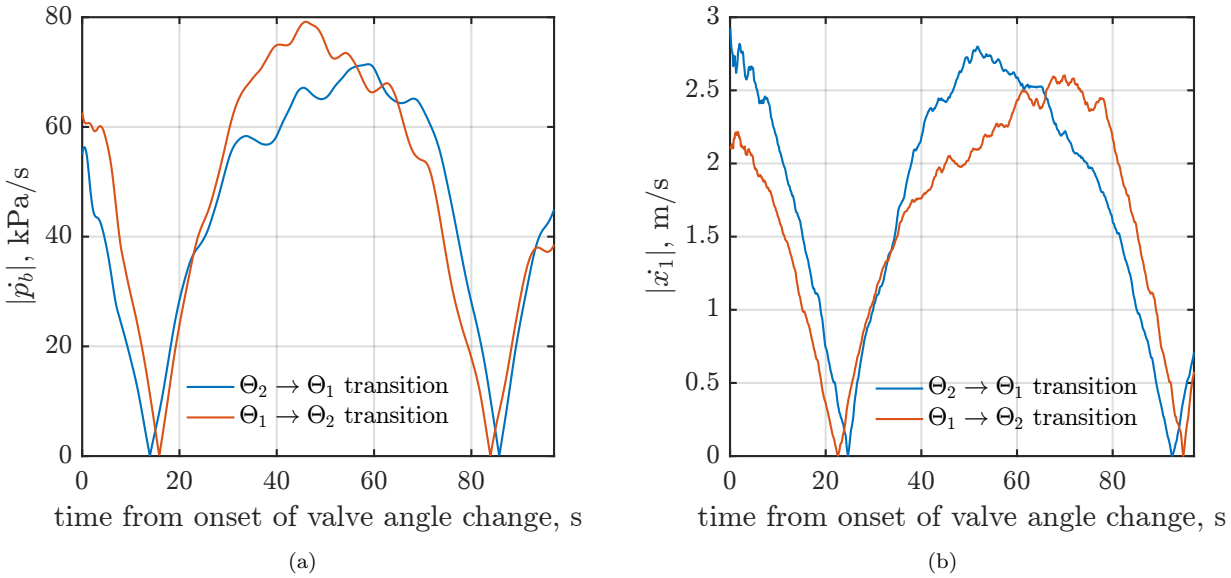

Figure 11. Time rate of change for different properties (run 18): (a) leading shock speed x_1; (b) back pressure rate of change $\dot{p}_b$.

Downloaded by UNIVERSITY OF MICHIGAN on April 5, 2018 | http://arc.aiaa.org | DOI: 10.2514/6.2017-0088

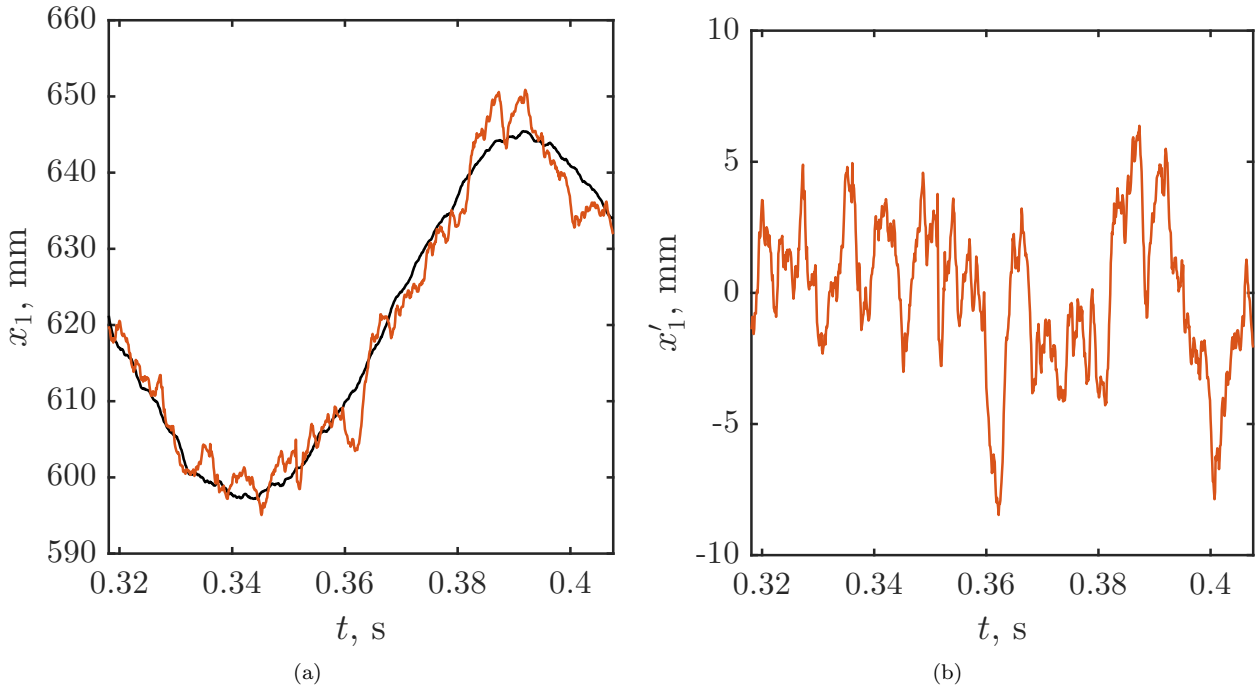

Figure 12. Example time traces (run 6): (a) comparison between the original time trace and the cycle-averaged curve; (b) fluctuation component found by subtracting the cycle-average from the original time trace.

Downloaded by UNIVERSITY OF MICHIGAN on April 5, 2018 | http://arc.aiaa.org | DOI: 10.2514/6.2017-0088

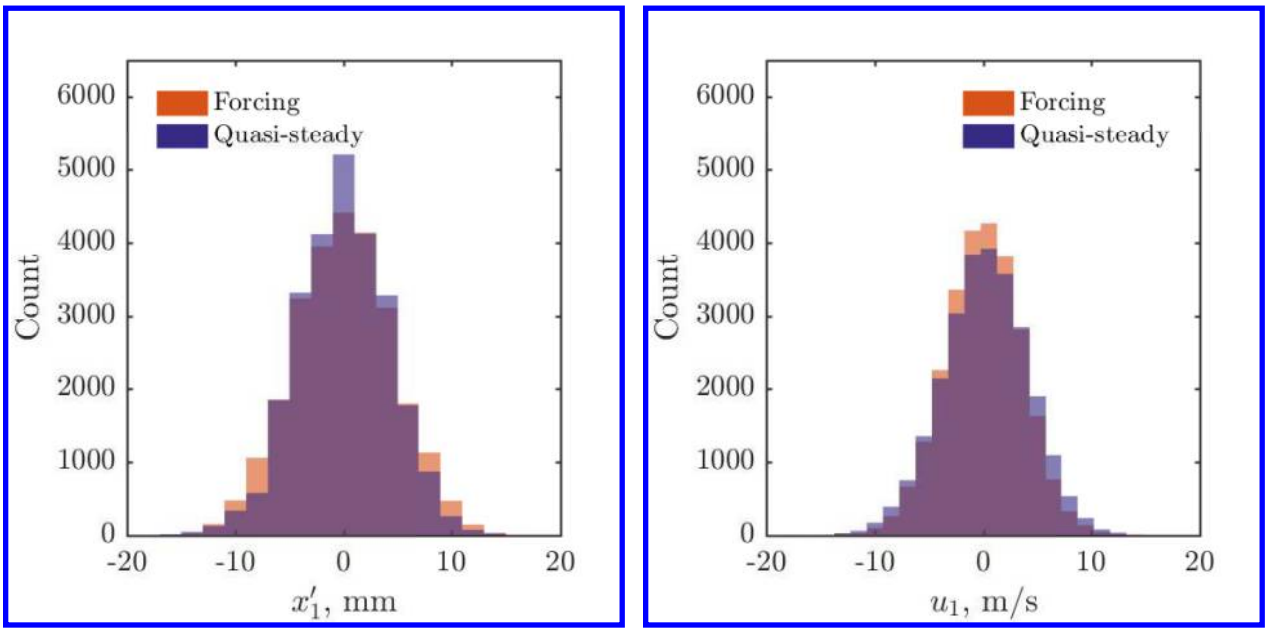

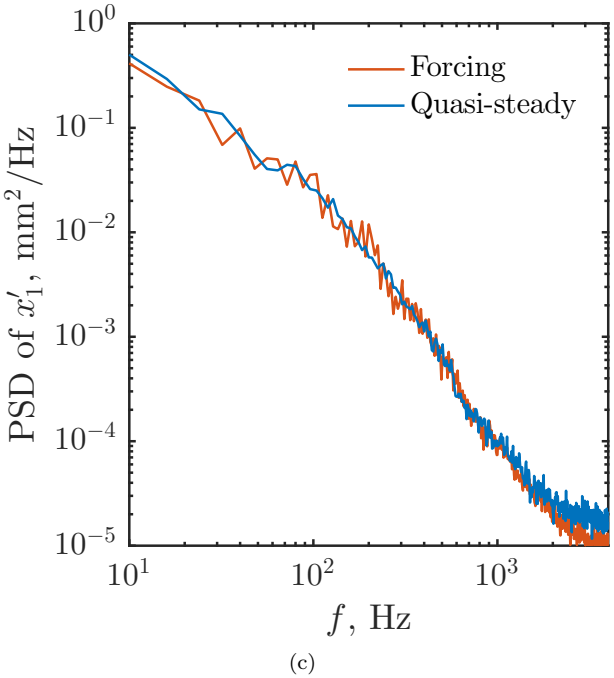

Figure 13. Example comparison of low-magnitude, high-frequency fluctuations during forcing and quasi-steady state (run 6): (a) histogram of x_1'; (b) histogram of u_1; (c) power spectral density of x_1'.

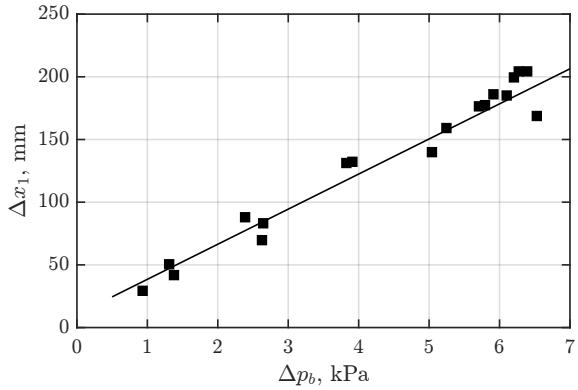

Figure 14. Leading shock displacement versus the magnitude of back pressure change.

Downloaded by UNIVERSITY OF MICHIGAN on April 5, 2018 | http://arc.aiaa.org | DOI: 10.2514/6.2017-0088

Downloaded by UNIVERSITY OF MICHIGAN on April 5, 2018 | http://arc.aiaa.org | DOI: 10.2514/6.2017-0088

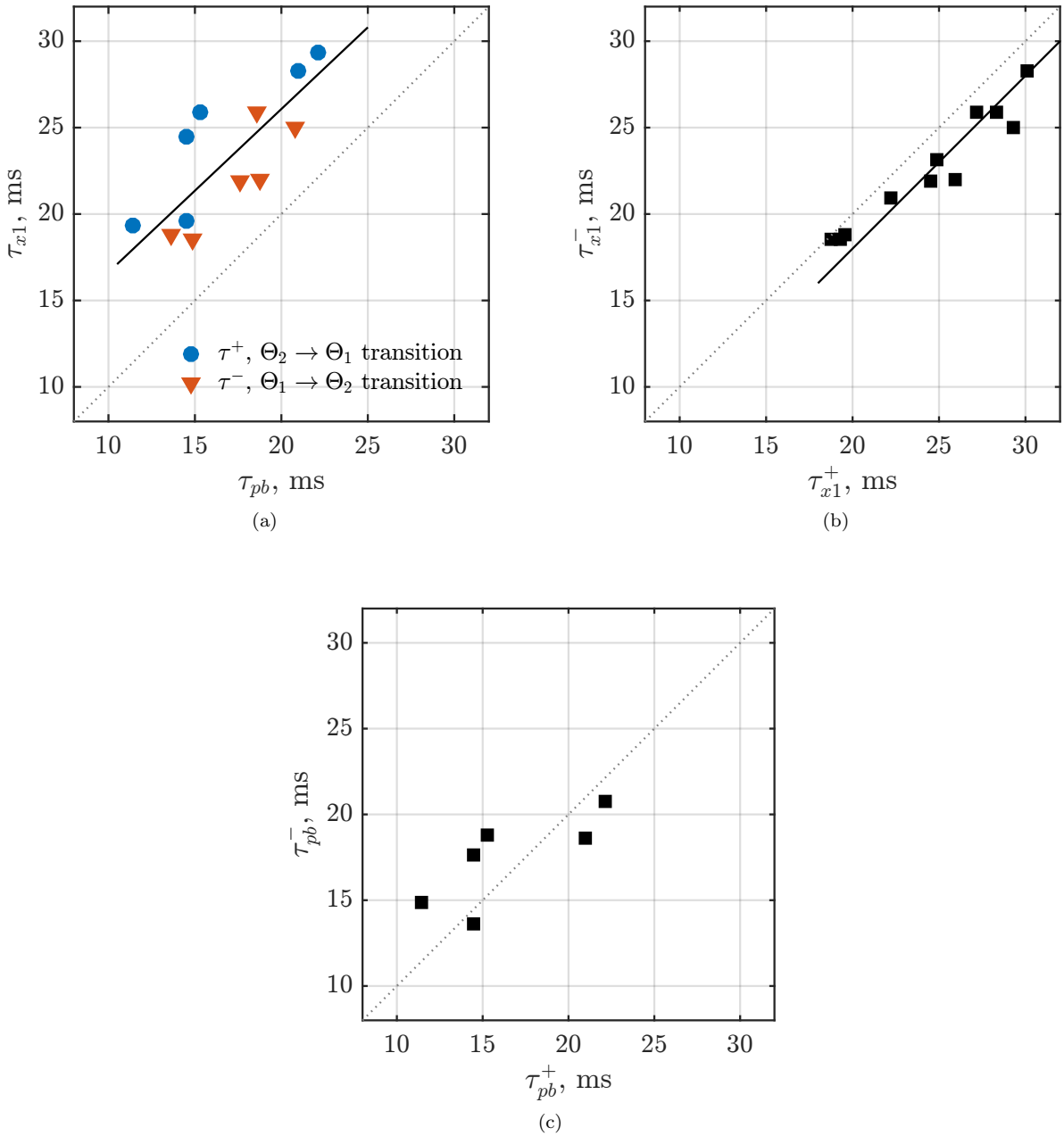

Figure 15. Time delays for runs with $\Omega > 2$ Hz: (a) time delay of leading shock position versus time delay back pressure; (b) comparison of leading shock time delay for different transitions; (c) comparison of back pressure time delay for different transitions.

Downloaded by UNIVERSITY OF MICHIGAN on April 5, 2018 | http://arc.aiaa.org | DOI: 10.2514/6.2017-0088

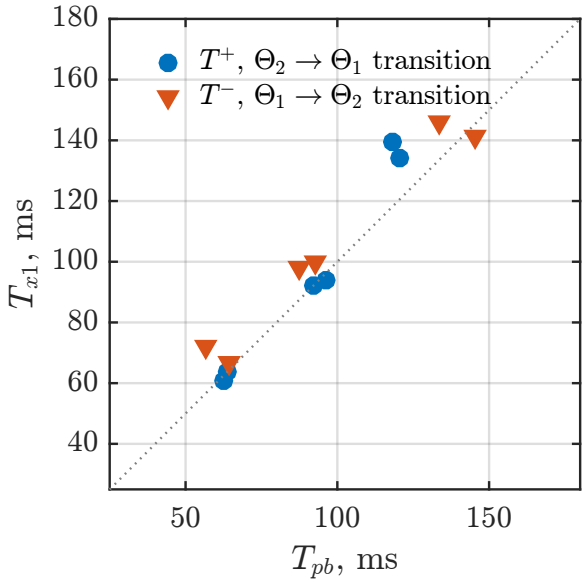

Figure 16. Rise time of leading shock position versus rise time of the back pressure for runs with $\Omega > 2$ Hz

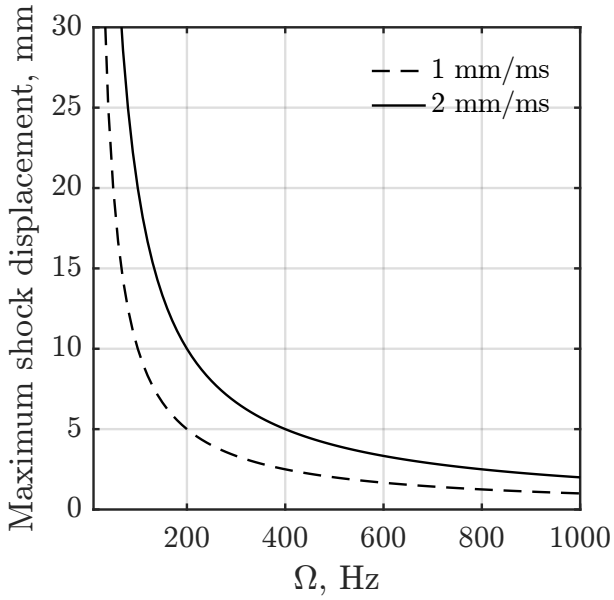

Figure 17. Extrapolated maximum shock train displacement for higher forcing frequencies.

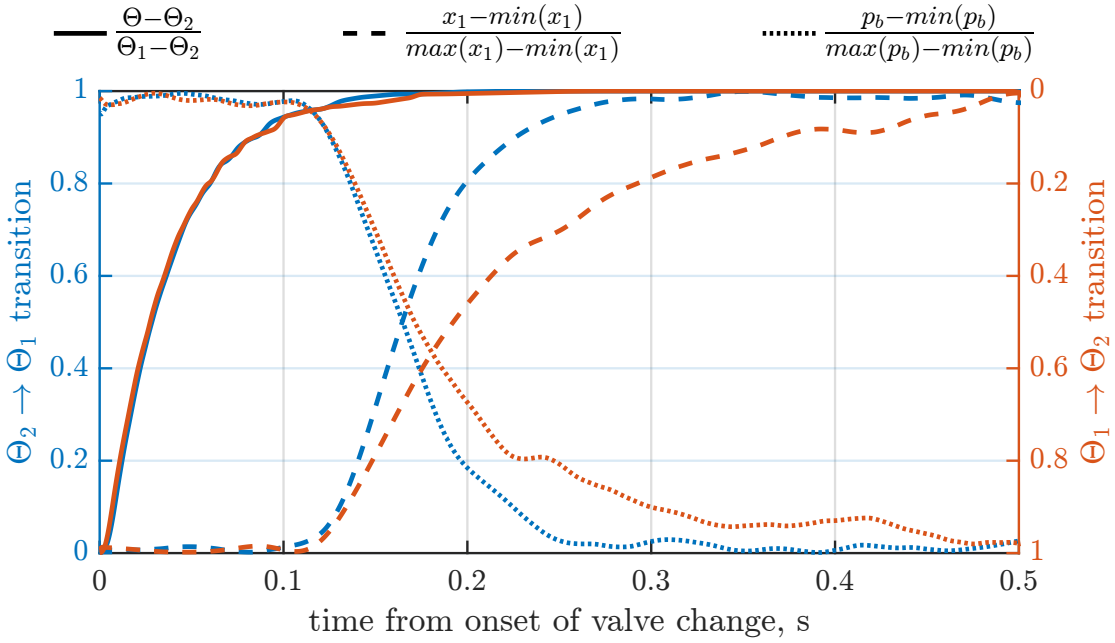

Figure 18. Normalized values of the cycle-average valve angle, shock position, and pressure during different transitions (run 19).

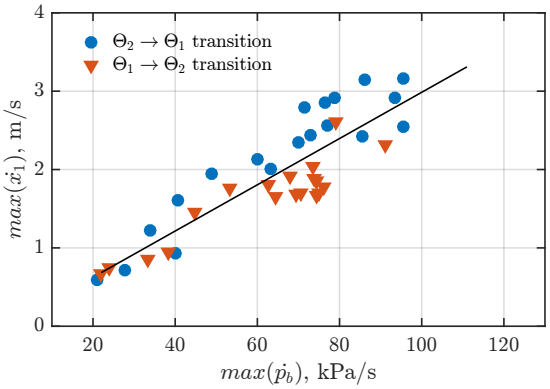

Figure 19. Maximum speed of the leading shock versus maximum back pressure rate of change.

Downloaded by UNIVERSITY OF MICHIGAN on April 5, 2018 | http://arc.aiaa.org | DOI: 10.2514/6.2017-0088

This article has been cited by:

1. Leon Vanstone, Joe Lingren, Noel T. Clemens. Supersonic Isolator Shock-Train Dynamics: Simple Physics-Based Model for Closed-Loop Control of Shock-Train Location . [Citation] [PDF] [PDF Plus]
2. Leon Vanstone, Kelley E. Hashemi, Joe Lingren, Maruthi R. Akella, Noel T. Clemens, Jeffrey Donbar, Sivaram Gogineni. Closed-Loop Control of Shock-Train Location in a Combusting Scramjet. *Journal of Propulsion and Power*, ahead of print1-8. [Abstract] [Full Text] [PDF] [PDF Plus]

Downloaded by UNIVERSITY OF MICHIGAN on April 5, 2018 | http://arc.aiaa.org | DOI: 10.2514/6.2017-0088